JOURNAL OF MATERIALS SCIENCE 13 (1978) 1249–1260

Effect of temperature and environment on crack propagation in graphite

S. W. FREIMAN, J. J. MECHOLSKY
Naval Research Laboratory, Washington, D.C., USA

Crack propagation studies were carried out on POCO AXF–5Q and ATJ–S graphite as a function of temperature and environment (for example H_2O, and CO and He). Crack growth rates in both graphites was essentially insensitive to the external environments at all temperatures. A transition from stable to catastrophic crack growth occurred at a particular temperature for each material. A definite effect of crack plane orientation with respect to the ATJ–S graphite billet was observed.

1. Introduction.

During ICBM re-entry into the atmosphere, graphite nose tips are subjected to temperature gradients of up to 2000° C or greater. These gradients produce thermal stresses in the centre of the nose tip which can cause crack growth, leading to failure. While the thermal stresses can be predicted using computer codes, and maximum initial flaw sizes can be predicted using a statistical approach, the existence of subcritical crack growth means that experimental determination of the parameters affecting slow crack growth must be made at the temperatures and environments of interest.

Previous work on various graphites indicates that fracture is both temperature and environmentally dependent [1–4]. These studies have demonstrated that: (1) if graphite is outgassed in vacuum prior to and during testing, its strength is significantly higher than when tested in air or other gases [1, 2]; (2) the strength of graphite generally increases with increasing temperature [1, 2]; (3) the temperature effect on strength disappears if the graphite is outgassed before testing, and (4) testing in H_2O can produce significantly lower strengths than testing in air [3].

The objective of this study was to determine the effects of temperature, environment and microstructure on crack propagation behaviour in graphite. A fracture mechanics approach was chosen for two primary reasons: (1) The material properties can be separated from the effects of a random flaw distribution in the material, and (2) the presence of stress corrosion induced, subcritical crack growth can be readily identified.

*Poco Graphite Co.
†Union Carbide Corp.

2. Experimental procedure

POCO AXF–5Q*, an isotropic, fine grained graphite (average grain size = ~ 7 μm) and ATJ–S†, an anisotropic graphite formed by pressing at temperature (grain size ~ 70 μm) were chosen for investigation because of their quite different microstructures. The elastic properties of both these materials as a function of temperature, which were used in the determination of fracture mechanics parameters, are given in Table I. Note that because of the anisotropic nature of an ATJ–S billet, there are two values of shear modulus which must be considered.

TABLE I Shear moduli of graphite in $N m^{-2} \times 10^{-10}$

Material	Temperature (° C)				
	21	1093	1371	1649	1927
POCO AXF–5Q	0.48	0.54		0.51	
ATJ–S transverse plane[a]	0.60	0.60	0.66	0.66	0.67
ATJ–S Isotropic plane[b]	0.44	0.50	0.58	0.59	0.60

[a]Measured by J. R. Koenig, Southern Research Institute.
[b]Calculated from values given by Starrett and Pears [5] based on the ratio of the G (transverse) measured on the present ATJ–S billet to that given in the reference.

2.1. Fracture mechanics test technique

A double torsion technique was used for the crack growth measurements, in which crack length is determined analytically from changes in the specimen compliance making visual observation of the crack

unnecessary. This test specimen was a plate of approximate dimensions 75 mm x 25 mm x 3.5 mm having a 1.75 mm deep groove down the length of the specimen to guide the crack. A characteristic of the geometry and loading of this specimen is that the driving force for crack propagation, i.e., strain energy release rate, G_I, is independent of crack length and is given by [6]:†

$$G_I = \frac{3P^2 W_m^2}{8t^3 t_1 WG[16/3 - 6.72(t/w)]} \quad (1)$$

Where G is the shear modulus in the direction of crack growth, P is the load, t the total specimen thickness, t_1 the thickness at the groove, W_m the distance between the load and support points and W the specimen width. The term in brackets corrects for non-linear effects arising due to larger thickness-to-width ratios. The more commonly used stress intensity factor, K_I, can be calculated from G_I as follows:

$$K_I = (G_I E^*)^{1/2} \quad (2)$$

where E^* is the effective modulus, such that

$$E^* = E = 2(1+\nu)G \quad (3)$$

for isotropic materials, e.g., POCO AXF–5Q, where E is the elastic modulus, ν is Poisson's ratio and G is shear modulus, and [7]

$$E^* = (2E_L E_T)^{1/2} \left[\left(\frac{E_T}{E_L}\right)^{1/2} - \frac{\nu_{LT} E_T}{E_L} + \frac{E_T}{2G_{LT}}\right]^{-1/2} \quad (4)$$

for anisotropic materials that are isotropic in a plane, e.g., ATJ–S graphite, where E_L is the elastic modulus transverse to the plane of the crack, E_T is the elastic modulus in the direction transverse to the load and ν_{LT} and G_{LT} are Poisson's ratio and shear modulus, respectively, in the plane perpendicular to the crack direction.

Evans [8] showed that under constant displacement or constant displacement rate, the crack velocity can be obtained from the load or the load relaxation rate. Because of the difficulty in separating inelastic compliance changes from those due solely to crack motion, the latter technique is being used in the study of graphite. Evans also showed that when the rate of head motion of the test machine, $\dot{y}$, is just compensated by the change in specimen compliance due to crack growth, the load becomes constant and crack velocity, V, is obtained from:

$$V = \frac{\dot{y} w t^3 G}{3PW_m^2} \quad (5)$$

As long as the displacement rate is significantly larger than the rate of inelastic processes in the material, any relaxation of the load due to these effects will be negligible. A constant load plateau is evidence that the crack is propagating and that the system can be considered as behaving elastically [8].

The test machine used in this study consisted of a servo-controlled hydraulic ram whose displacement rate is controlled by a digital ramp generator giving displacement rates from approximately 10^{-8} to 10^{-3} m sec^{-1}. Measuring crack velocities at rates lower that 10^{-8} m sec^{-1} proves difficult due to both relaxation of the specimen as well as to drift in the test machine. The specimens were loaded using steel loading platens in which SiC loading pins had been inserted. The stiffness of the load train was calculated to be much higher than that of the specimen. The output of a load cell as plotted on a strip chart recorder was used to calculate both G and V.

2.2. Environmental testing system

A transparent plastic cover resting on the steel base containing the hydraulic ram provided a chamber for atmosphere control, e.g., of both relative humidity‡ and oxygen content§ (Fig. 1). Before testing in other atmospheres, the specimens were placed in the chamber, which was then purged with an inert gas (He or N_2) and held under a slight positive pressure of the inert gas during testing. Normal oxygen contents of 1 to 2% and relative humidities in the 6 to 10% range were recorded, although, as discussed later, variations from these levels seemed to have no effect on crack growth behaviour. In the case of the carbon monoxide (CO) environment, the gas was directed down the specimen during testing using a flexible hose. Data in H_2O was obtained by immersion in a water filled steel pan attached to the lower loading ram.

†It has been shown that this loading does yield the opening mode value of G, i.e., G_I.

‡Beckman Inc., Model 1715.

§Panametrics Inc.

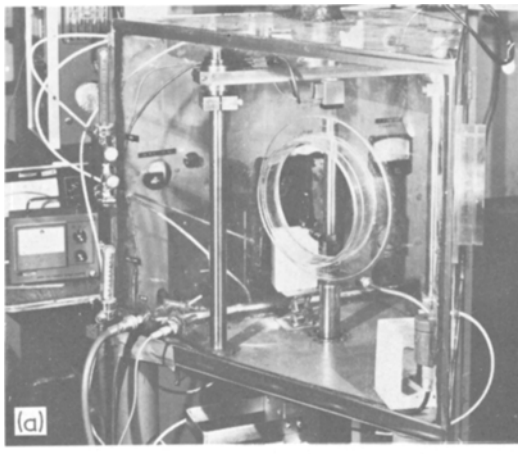

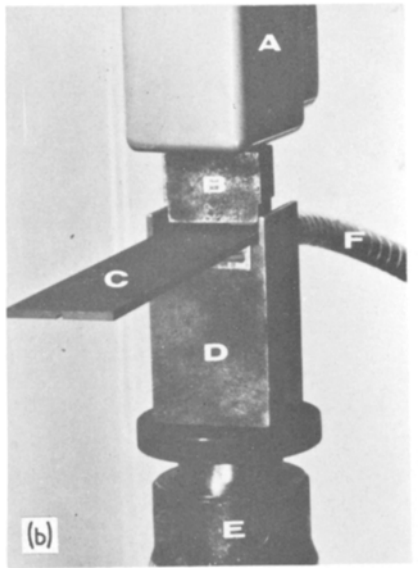

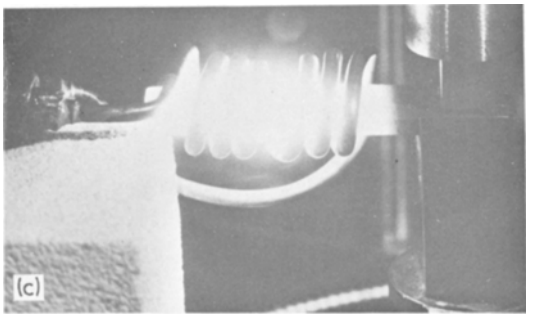

Figure 1 Environmental test system used for crack growth experiments. (a) Plexiglas test chamber; induction furnace in background. (b) Loading system showing load cell (A), loading platens (B and D), graphite specimen (C), loading ram (E), and CO inlet hose (F). (c) Loaded graphite specimen being heated in induction coil.

Elevated temperatures in the graphite specimens were attained by making the specimen the susceptor in an induction heating system.* Fairly uniform heating over the specimen length within the coil, as measured using an optical pyrometer, was achieved. Because the specimens were relatively thin, $\approx$ 3.5 mm, it was assumed that heating through the thickness would also be quite uniform. The temperature at the specimen surface was monitored using an optical pyrometer, sighting through the induction coil, and the millivolt readout recorded simultaneously with load in a dual pen strip chart recorder. Temperatures up to $\sim$ 1900° C were achieved, with limitations to higher temperatures being simply the efficiency of the coil design.†

Specimens were heated to the desired temperature in times of 20 to 30 sec. Some outgassing of the graphite was observed during heating up. Loading was generally begun just before the desired temperature plateau was reached. In most cases, especially for tests conducted at the slower rates, the specimen remained at a constant temperature for 10 to 30 sec before crack propagation occurred. It was assumed that the specimen had equilibriated at the given temperature. The validity of this assumption is borne out by data taken after 5 min holds at temperature, which was within the range of that taken immediately upon reaching temperature. Fracture surfaces were examined in both the SEM and the TEM, employing carbon-shadowed plastic replicas for the latter.

3. Results and discussion

3.1. POCO AXF–5Q

Fig. 2 shows the crack propagation (V versus G_I) data for POCO AXF–5Q graphite in air, H_2O, N_2 and CO at 20° C plotted on a log–log scale.

First, note there is a definite stable crack growth (slope, $n = 28$) phenomenon akin to that observed in many other ceramics. Second, note that no difference in behaviour could be observed in the various environments, implying that external environment has little effect on the mechanism of crack growth.

As seen in Fig. 2, the data obtained in this study lies at lower G_I values and has a different slope than that of Hodkinson and Nadeau [9]. However, their data was obtained by loading a

*Cycledyne Inc.

†High temperatures are easy to achieve by increasing the size of the sample; however, the analysis used for the fracture mechanics test is no longer valid because of the increased thickness of the specimen.

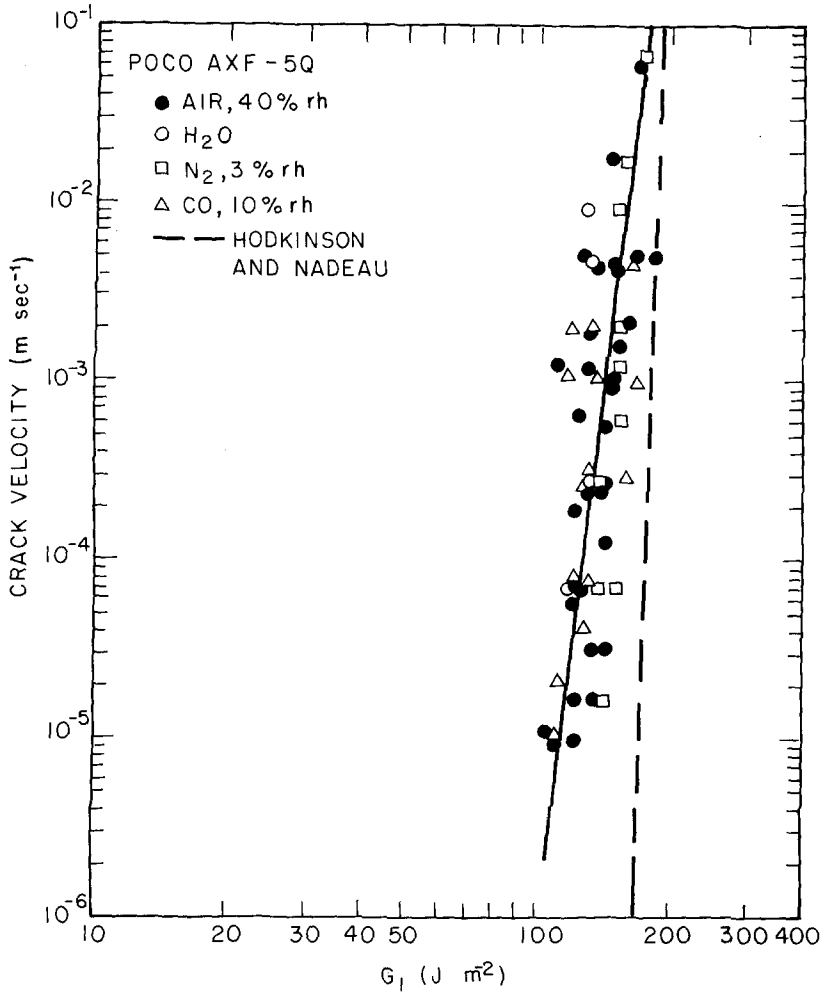

Figure 2 Crack velocities as a function of G_I for POCO AXF–5Q tested in various room temperature environments. Data is compared to that of Hodkinson and Nadeau [9] (dashed line).

double torsion specimen using a load relaxation technique. It is possible that all of the non-elastic deformation in the specimen was not accounted for in their case, which would lead to calculation of higher G_Is.

The effect of testing at elevated temperatures (1200 to 1700° C) on crack growth in POCO AXF–5Q is shown in Fig. 3 along with the best fit straight line representing all of the 20° C data. The data obtained in air at crack velocities approaching 10^{-4} m sec^{-1} falls in the range of that at room temperature with the deviation to large G_I increasing with increasing loading rate. This data suggests a transition in behaviour with temperature and loading rates, although subcritical crack growth was observed at all times. In He, a transition in behaviour between room temperature and 1700° C occurs, as illustrated by the change in the loading curve in Fig. 4. Behaviour at room temperature corresponded to that observed in other environments (i.e., a load plateau); at 800 to 1100° C, the shape of the load–time curve suggests that the crack initially grows in a stable manner (at a higher G_I than at room temperature) but quickly accelerates to a very high velocity. Above about 1200° C rapid fracture of the specimen occurs at a G_I of 280 to 300 Jm^{-2} with no evidence of any subcritical crack growth. The increased slope of the curves at elevated temperatures is due to the greater specimen stiffness (larger G). The crack velocities in Fig. 3, for He at 1200 to 1700° C were calculated from the displacement rate of the loading head $\dot{y}$, and the maximum load observed, even though only sudden fracture occurred, in order to demonstrate the point that the G_I at which critical crack growth took place was independent of loading rate.

It appears that stable crack propagation behaviour observed at room temperature occurs due to a stress-corrosion type process, analogous to that in other ceramics, the active species being gases already absorbed in the graphite. Tempera-

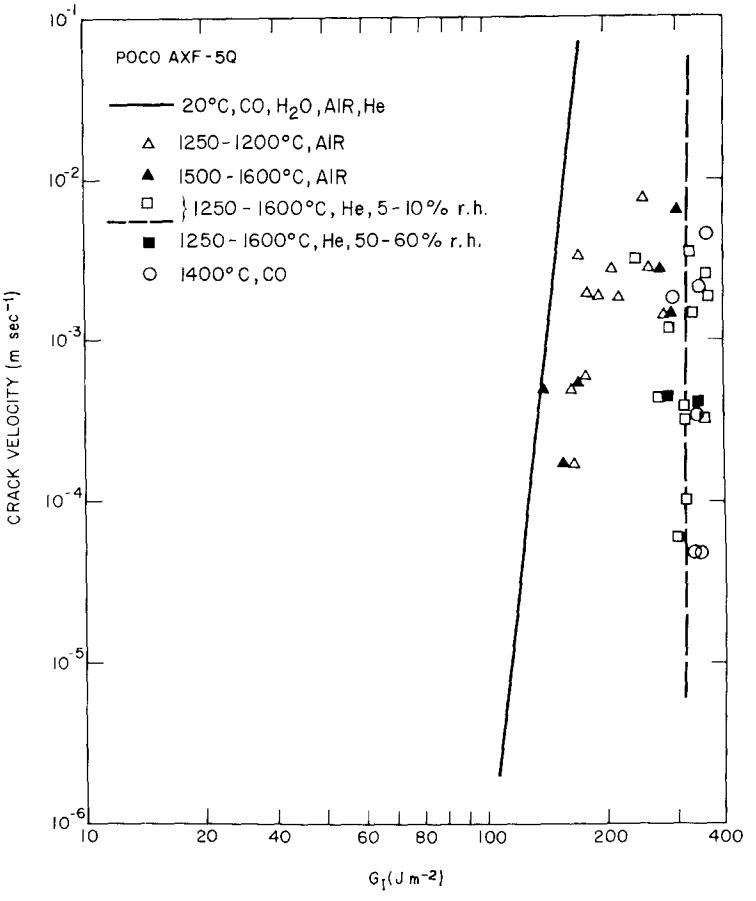

Figure 3 Crack velocities as a function of G_I for POCO graphite tested at both ambient and elevated temperatures indicate no subcritical crack growth. The velocities represent displacement rates at which catastrophic crack growth occurred.

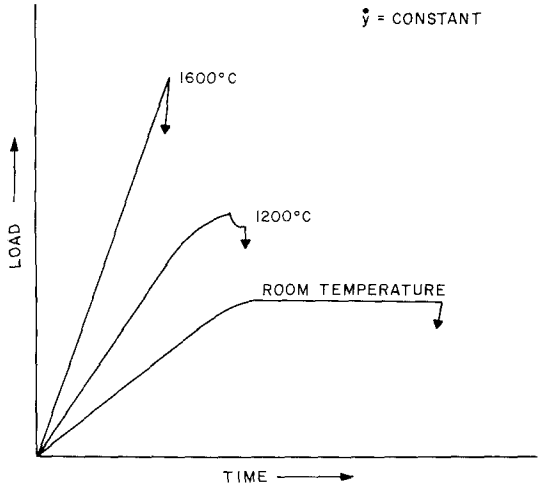

Figure 4 Change in shape of loading curve demonstrating transition from stable crack growth to catastrophic failure.

tures of 500° C are in the range at which water is first given off by graphite.* It has been observed that almost all of the H_2O is gone above 800 to 1100° C [10]. Data observed under flowing CO at elevated temperatures also fell in the scatter band of that obtained in Fig. 3.

A limited number of experiments were performed in which the He was bubbled through H_2O before it entered the test chamber. This yielded relative humidities of 50 to 60% compared to the usual 5 to 6% for He. No difference in crack propagation behaviour was observed, so that either the quantity of H_2O available at the crack tip was too small or no absorption of H_2O would occur at these temperatures. Specimens heated to ~1700° C in He, held there for 90 sec, then cooled slowly to room temperature before testing showed no difference in behaviour from the as-received specimens tested at room atmosphere, suggesting that gases absorbed by the graphite on cooling were sufficient to produce stress corrosion. Since gases are already present in the graphite, external gaseous environments would be expected to have little effect on crack propagation, as observed. At high temperatures, these gases would be purged from the graphite so that no stable crack growth occurs. This behav-

*This is consistent with the observation of vapours given off when graphite was heated in He as well as the simultaneous increase in the relative humidity of the chamber.

iour is consistent with the increases in strength observed on the degassing of graphite [1, 2].

While there appeared to be differences between the fracture surfaces obtained under different conditions, the fine grain size of the POCO graphite made identification of specific changes in fracture patterns quite difficult. Transmission electron micrographs of fracture surfaces of POCO graphite tested in air and He at both 20° C and 1600° C showed two primary points.

(1) Failure under all of the above conditions was primarily transgranular. Fine grained areas that appeared intergranular at low magnifications in the SEM were identified as transgranular at higher magnification.

(2) Observation of a large number of micrographs indicate that there is at least a qualitative difference in fracture topography of specimens tested above and below 1300° C, although these are difficult to detect.

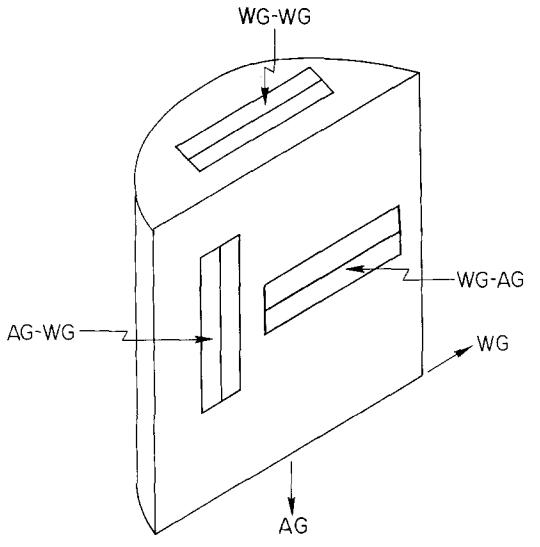

Figure 5 Schematic of double torsion specimen orientations with respect to with grain and across-grain (pressing) direction in an ATJ–S graphite billet.

3.2. ATJ–S

Because billets of ATJ–S graphite are made by pressing, the graphite lamellae tend to lie with their easy cleavage planes perpendicular to the pressing direction. The material is transversely isotropic, the lamellae being randomly oriented in the transverse plane. This type of anisotropy means that there are three different specimen orientations (Fig. 5). Designation of ATJ–S specimens is given by codes which specify the orientation, e.g., AG–WG (Across Grain–With Grain), the first two letters being the crack propagation direction, the second the direction of the principal tensile stress at the crack tip.

The 20° C crack propagation data for the three orientations of ATJ–S graphite are given in Figs. 6 to 8. Best fit straight lines were drawn through the combined air, CO and He data. Of all the environments in which tests were run, e.g., air, CO, He, H_2O, only the latter had any apparent effect on the crack propagation rate. The relative position of the V–G_I curve for each orientation is that expected based on the orientation of the graphite lamellae with respect to the crack plane. In the WG–AG orientation, a sizeable proportion of graphite grains are oriented so that the interlamellar plane is the same as that of the crack. Since the bonding across this plane is a minimum, the resistance to crack propagation should be the smallest, as observed. In the AG–WG orientation most of the grains will be oriented such that the crack must cut the grain by breaking bonds in the plane of the graphite lamellae or travel around the grain, both of which require high energies. In the WG–WG orientation, the crack must also cut graphite grains, but the grain profile presented to the crack should be much smaller than in the AG–WG orientation making crack path deviation energetically more feasible.

Scanning electron fractography (Fig. 9) demonstrated that each of the three orientations of ATJ–S graphite has a distinctive fracture surface associated with it. The AG–WG orientation (crack propagating across the grains and loaded in the with-grain plane) predominantly leaves "books" or edge stacks of grains as evidence of propagation through or around the grain stacks. This type of fracture should be the most difficult since graphite planes are being fractured in their strongest direction, in agreement with the V–G_I data (Fig.7). The WG–AG orientation leaves evidence of transgranular fracture across the grains (and some grain stacks due to misorientation of graphite lamellae with respect to the with-grain plane, Fig. 9). It would be reasonable to assume that this is the weakest orientation since the crack separates many of the graphite planes in the direction of weakest bonding. The fracture surface of the WG–WG orientation does not leave as distinctive markings as the WG–AG orientation, but there is evidence of the crack front deviating around the stacks of graphite lamellae and occasionally cleaving these stacks, so that in some areas one would expect

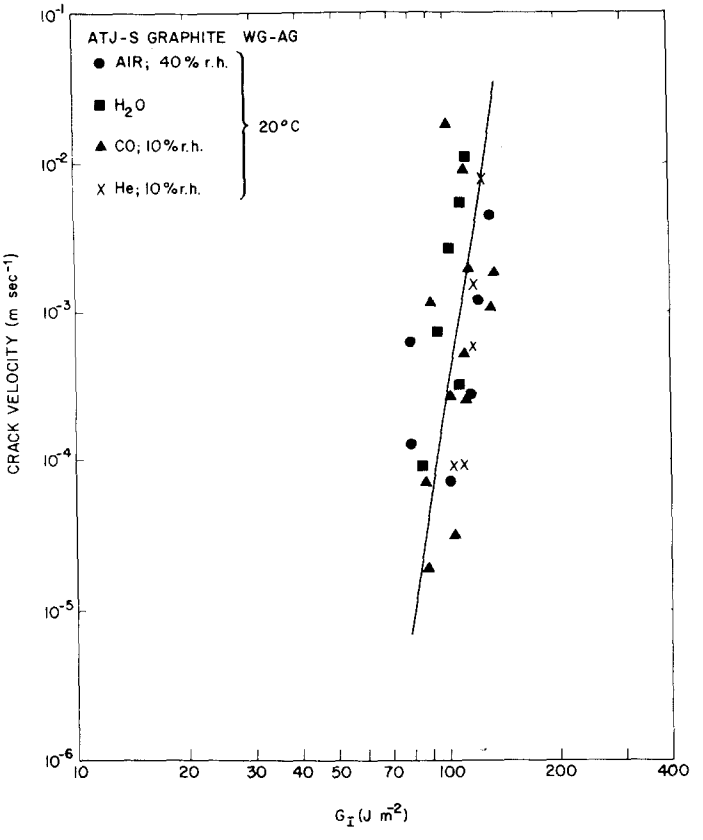

Figure 6 Crack velocities as a function of G_I for ATJ–S graphite (WG–AG orientation) tested in various environments at 20° C. Line represents least squares fit to the data in air.

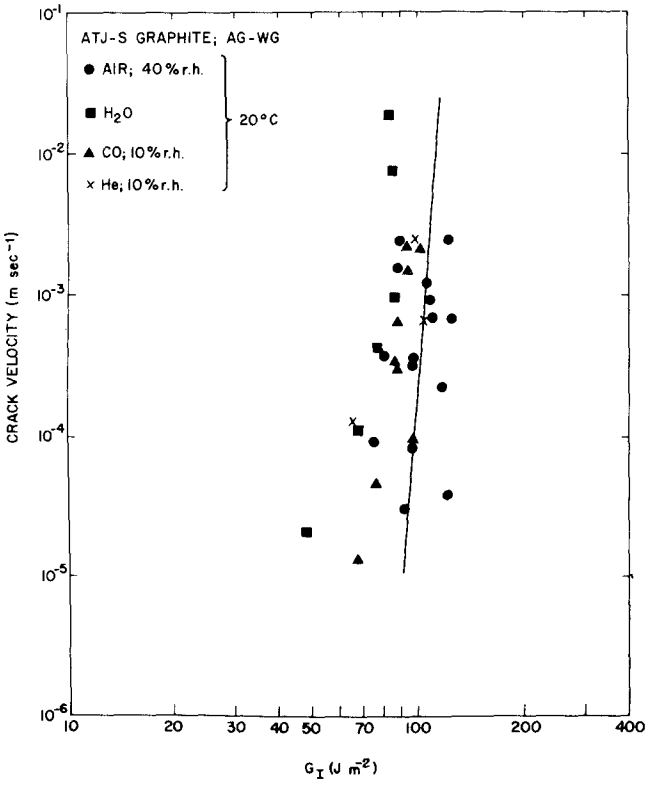

Figure 7 Crack velocities as a function of G_I for ATJ–S graphite (AG–WG orientation) tested in various environments at 20° C. Line represents least squares fit to the data in air.

similar microstructure as observed in the AG–WG orientation. The results of this fracture surface analysis shows that transgranular fracture predominates ATJ–S failure in the WG–AG direction, and probably a mixed-mode failure governs the WG–WG orientation.

The crack propagation data in ATJ–S obtained at elevated temperatures is plotted as crack velocity versus G_I (Figs. 10 to 12) along with the best fit straight lines representing the 20° C data. The overall increase in crack growth resistance with temperature is smaller in ATJ–S than in POCO AXF–5Q graphite. However, it does appear that data obtained in all environments at ~ 1300 to 1500° C generally lie at higher G_Is for the WG–AG orientation. The data for the WG–AG and AG–WG overlaps considerably at these temperatures. Unlike POCO AXF–5Q, stable crack growth in He and CO was observed at least below a crack velocity of 10^{-2} m sec^{-1}. In order to determine whether the extent of outgassing at a particular temperature would influence the crack propagation behaviour, several specimens were held at temperature in He for approximately 5 min before testing, instead of the 30 sec to 1 min used for most specimens. It was observed that the hygrometer reading increased significantly during this 5 min period, implying an increase in the amount of water vapour in the chamber. However, because the hygrometer may also be sensitive to other gases such as short chain length hydrocarbons, no absolute conclusions can be drawn. The V–G_I data for these specimens were no different from those of the majority for specimens tested in He at elevated temperatures. Little difference in the V–G_I curves was also observed between ≈ 1000 and 1700° C (Figs. 10 to 12); at ≈ 1700° C stable crack growth ceased, only sudden failure being observed. This behaviour strongly suggests an environmental behaviour similar to that in the POCO AXF–5Q, the difference being that the transition to sudden failure occurs at a much higher temperature in the ATJ–S. The fracture surfaces of the specimens tested at elevated temperatures (1000 to 1900° C) showed little or no difference from the surfaces at 20° C for all orientations.

As has been pointed out previously, the crack propagation data could equally be plotted as velocity versus K_I instead of G_I, where K_I for anisotropic material such as ATJ–S is given by Equations 2 and 4. By comparing both G_I and K_I for-

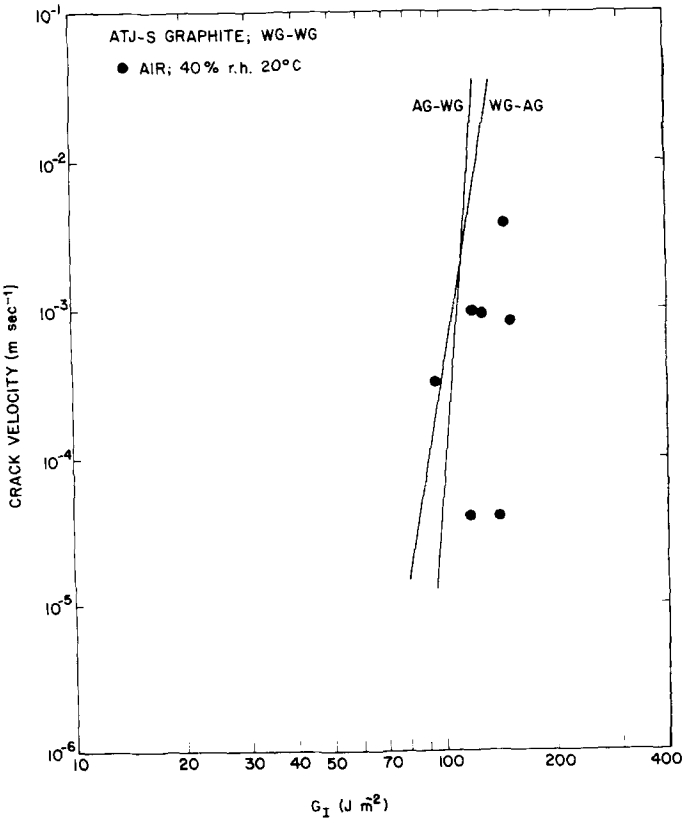

Figure 8 Crack velocities as function of G_I for ATJ–S graphite (WG–WG orientation) tested in air at 20° C. Lines are from Figs. 6 and 7, and due to data scatter, these curves are not significantly different.

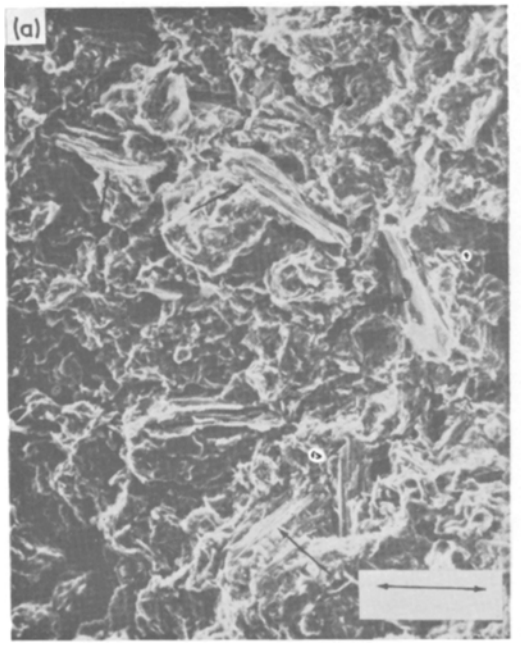

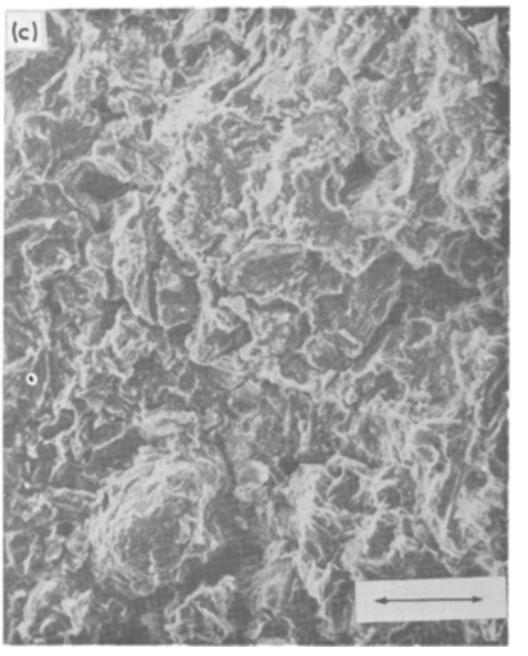

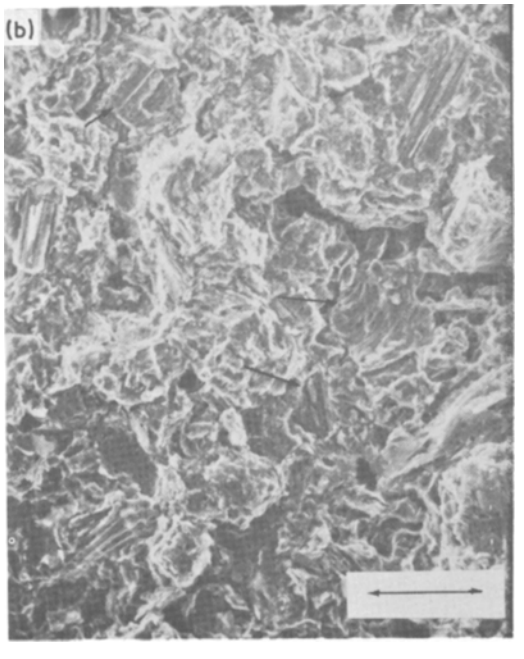

Figure 9 Fracture surfaces of ATJ–S graphite tested at 20° C. (a) AG–WG, arrows denote "books" or edges of grains. (b) WG–AG, arrows point to large, flat cleavage faces. (c) WG–WG, mixture of (a) and (b).

mulations, the effect of temperature on the crack propagation resistance may be separated from the effect of the modulus.

The V–K_I data for ATJ–S at 20° C and ~ 1400° C (in He) are compared in Fig. 13. This was plotted on a semi-log plot for clarity because this gives more spread in the data. On this basis, one would say that crack propagation in the AG–WG orientation is the least affected by temperature and environment while the WG–AG is affected the most, and the WG–WG intermediate to the other two. This is not unexpected since the greatest effect of environment should occur on fracture between the graphite lamellae (WG–WG) while fracture across a filler particle (AG–WG) should be relatively insensitive to environment. The only difference in the relative order of the orientations is the AG–WG and occurs due to the large change in modulus in the AG direction with temperature (0.38 to 0.48 × 10^4 MN m^{-2}, Table I).

4. Conclusions

(1) There is no effect of external environment (H_2O, CO, air, He) on crack growth rates in POCO AXF–5Q or ATJ–S graphite at any temperature.

(2) A transition from stable to catastrophic crack growth takes place at ≈ 800° C in POCO and 1600° C in ATJ–S graphite. This transition is interpreted to be due to the complete elimination of H_2O vapour from the graphite at the particular temperature, thereby removing the stress corrosion agent.

(3) A definite effect of crack plane orientation with respect to the pressing direction in ATJ–S was observed. The most resistant orientation is

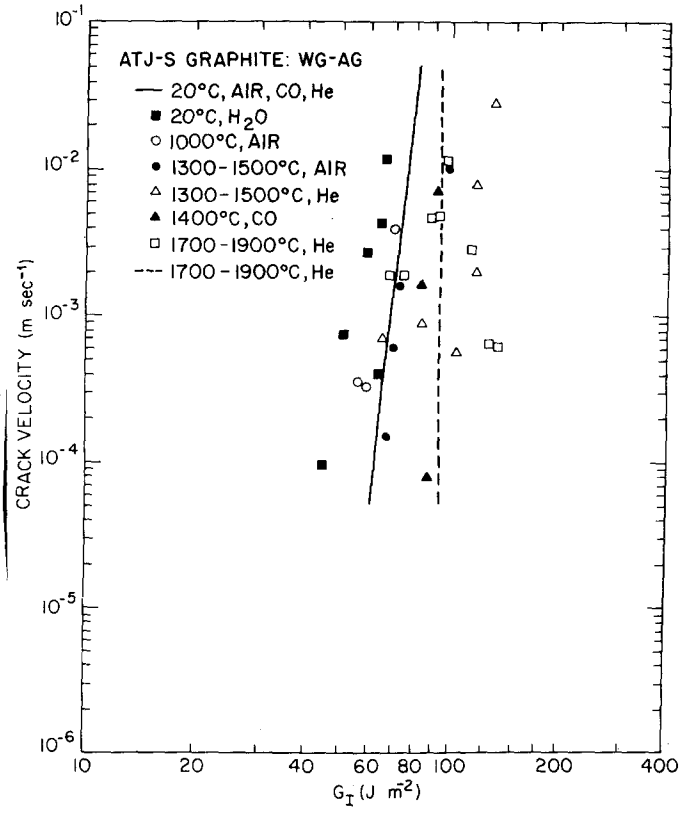

Figure 10 Crack velocity as a function of G_I for ATJ–S graphite (WG–AG orientation). Solid line is least squares fit to 20° C data. Dashed line indicates no subcritical crack growth at ≃ 1700° C in He.

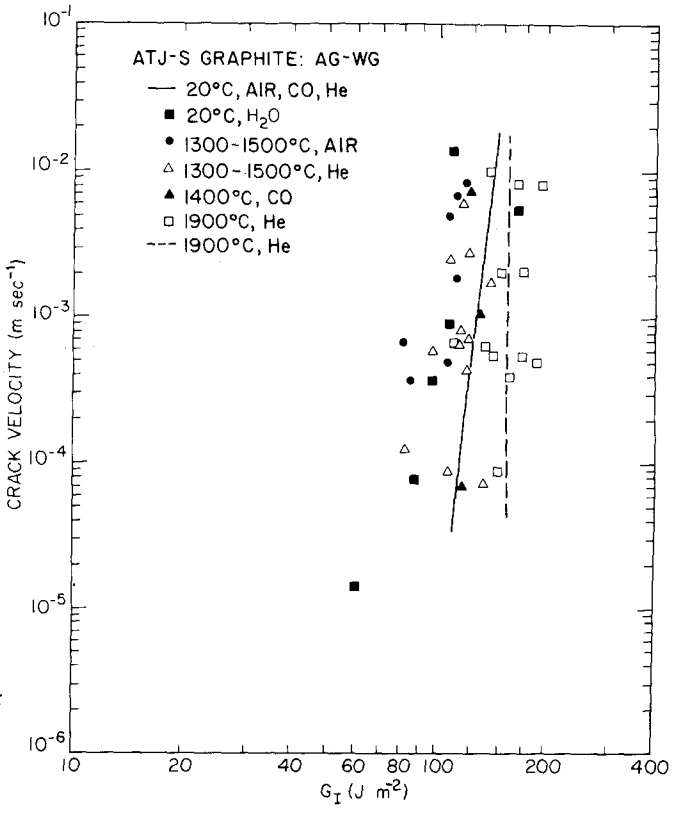

Figure 11 Crack velocity as a function of G_I for ATJ–S graphite (AG–WG orientation). Solid line is least squares fit to 20° C data. Dashed line indicates no subcritical crack growth at ≃ 1700° C in He.

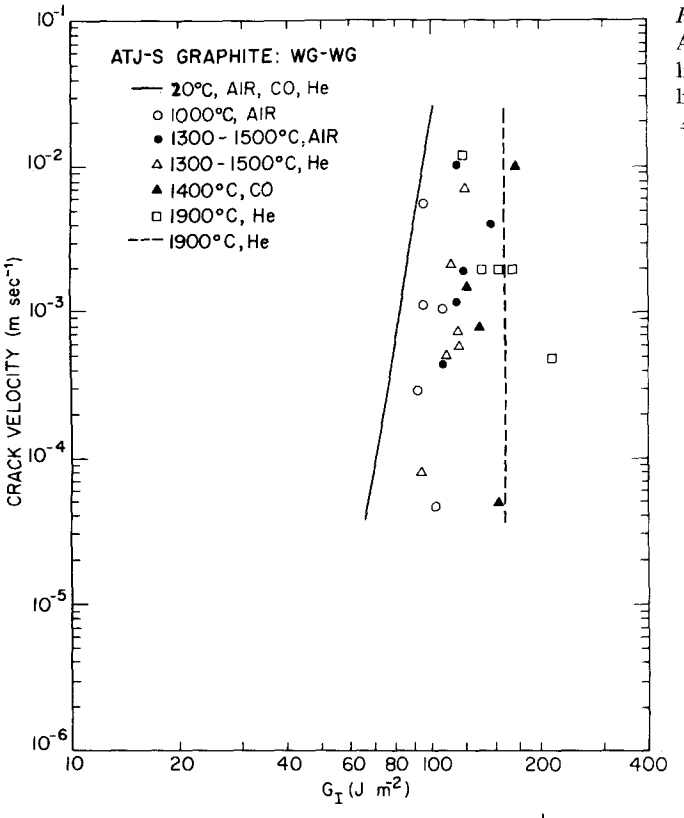

Figure 12 Crack velocity as a function of G_I for ATJ–S graphite (WG–WG orientation). Solid line is least squares fit to 20° C data. Dashed line indicates no subcritical crack growth at $\simeq$ 1700° C in He.

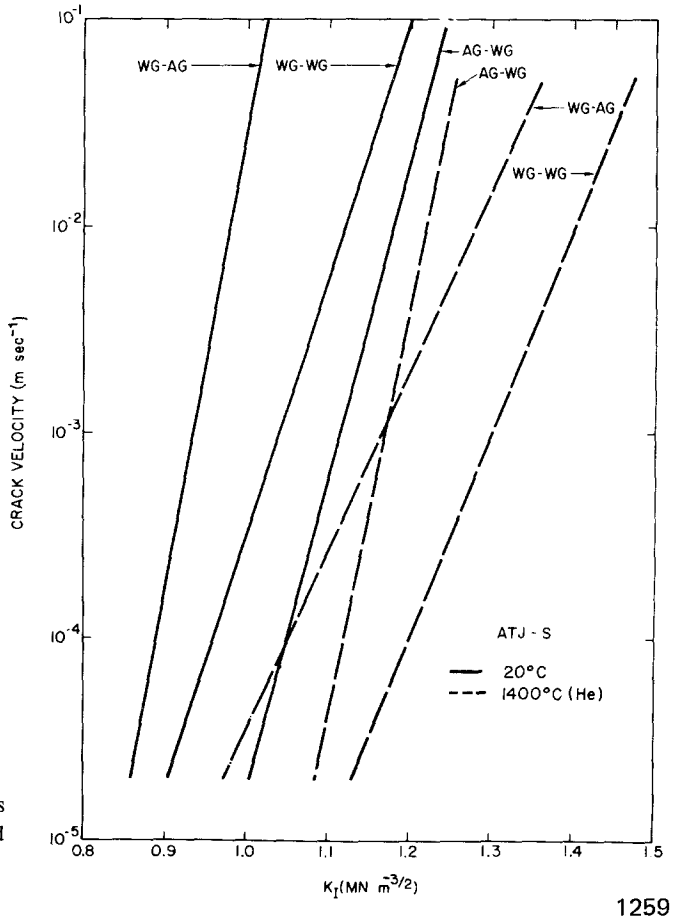

Figure 13 Crack velocity as a function of stress intensity K_I, for ATJ–S graphite at 20 and 1400° C.

that in which the crack propagated in the pressing direction, perpendicular to the graphite lamellae, while the weakest was that in which the crack propagated between the lamellae.

Acknowledgements

The authors would like to acknowledge the aid of P. Miller in carrying out the crack growth experiments and J. Robinson and Dr W. H. Cullen who contributed to the fractographic studies. The financial support of the Naval Surface Weapons Centre, White Oak, is gratefully acknowledged. We would also like to thank the Contract Monitors, R. Goderstad and D. Rester, for their help in this study.

References

1. R. J. DIEFENDORF, Proceedings of the Fourth Biannual conference on Carbon (1961) 489.
2. G. W. ROWE, *Nucl. Eng.* (1962) 102.
3. F. H. VITOVEC and Z. H. STACHURSKI, *Carbon* **10** (1972) 417.
4. L. R. HETTCHE and T. R. TUCKER, "Cracks and Fracture," STP 601, ASTM (1976).
5. H. S. STARRETT and C. D. PEARS, "Probable and Average Properties of ATJ–S (WS) Graphite," Technical Report No. AFML–TR–73–14, Vol. I (1973).
6. K. R. McKINNEY and H. L. SMITH, *J. Amer. Ceram. Soc.* **56** (1973) 30.
7. P. C. PARIS and G. C. SIH, "Fracture Toughness Testing and Its Applications," STP 381, ASTM (1964).
8. A. G. EVANS, *J. Mater. Sci.* 7 (1972) 1137.
9. P. H. HODKINSON and J. S. NADEAU, *ibid.* **10** (1975) 846.
10. R. A. MEYER, Aerospace Corporation, private communication (1976).

Received 31 August and accepted 1 November 1977.